



High-temperature superconductivity in monolayer FeSe on SrTiO₃ and related systems mediated by low energy plasmons

Tong Wei  and Zhenyu Zhang *

International Center for Quantum Design of Functional Materials (ICQD), Hefei National Laboratory for Physical Sciences at Microscale (HFNL), and CAS Center for Excellence in Quantum Information and Quantum Physics, University of Science and Technology of China, Hefei, Anhui 230026, China



(Received 16 July 2021; revised 6 September 2021; accepted 28 September 2021; published 9 November 2021)

The dominant mechanism of high-transition-temperature (T_c) superconductivity in cuprates remains an agonizing puzzle in condensed matter physics. The more recent discoveries of FeSe-based superconductors provide ideal new platforms to explore the high- T_c superconducting mechanism. Here we develop a generic mechanism of superconductivity centered at the commonality shared by many high- T_c materials, namely, their effective carrier densities are universally low, and are therefore necessarily accompanied by low energy plasmons. We first show that the excitations of such plasmons can largely suppress the Coulomb repulsion of the electrons. Furthermore, the electron-phonon and electron-plasmon couplings can inherently join force in mediating electron pairing, and when applied to the monolayered FeSe on SrTiO₃, the plasmon-enhanced T_c is one order of magnitude higher than that due to phonon alone, to the experimentally observed range. The present “phonon + plasmon” mechanism also embodies characteristic dependences of T_c on the carrier density and isotope substitution, and may find broad applicability in many superconducting systems with low carrier densities, including, most notably, the cuprates.

DOI: [10.1103/PhysRevB.104.184503](https://doi.org/10.1103/PhysRevB.104.184503)

I. INTRODUCTION

Beyond their preceding counterparts of cuprates [1–3], iron-based superconductors have attracted tremendous attention as a new and fertile ground for exploring microscopic mechanisms of high- T_c superconductivity [4–12]. Most strikingly, it has been observed that the T_c in unit-cell FeSe grown on SrTiO₃ (1uc-FeSe/STO) can be dramatically enhanced from that of bulk FeSe [7–10], surpassing the expectation of the standard BCS theory with conventional electron-phonon coupling (EPHC) [13]. Consequently, other bosonic modes or exotic mechanisms have been actively pursued to explain the enhanced electron pairing, including spin fluctuations [14–17] and interfacial polarons [18]. Despite these extensive efforts, the dominant microscopic mechanism of enhancement remains under active debate [19–22]. Needless to say, what is really responsible for the high- T_c in cuprates remains as an even more agonizing puzzle.

In searching for likely enhancement mechanisms of high- T_c superconductivity in Cu- or Fe-based systems, a pronounced feature to emphasize is the sensitively tunable T_c via carrier doping [2,3,10]. However, even at the optimal doping defined by the highest T_c , the effective carrier densities remain low [2,3,9,10]. Such low carrier densities are typically accompanied by large Coulomb repulsions in the systems, resulting from the less effective screening and weaker retardation within the BCS picture [23,24]. On the other hand, the low carrier densities are also necessarily accompanied by

plasmons whose energies are as low as the typical phonon modes invoked in the electron pairing via the EPHC mechanism, as explicitly shown for the 1uc-FeSe/STO system [16,18,25–35]. Yet to date, whereas the role of phonons in electron pairing has been well accepted [13], that of plasmons as a bosonic mode in mediating electron pairing via electron-plasmon coupling (EPLC) has been relatively less investigated [36–39], especially for the iron-based high- T_c superconductors. In particular, the potential synergistic effect of EPHC and EPLC in enhancing superconductivity, as treated in several other systems [37,38,40–43], has never been considered for 1uc-FeSe/STO, and this treatment is the primary objective of the present study.

In this study, we perform the first treatment on the crucial role of low energy plasmons in enhancing electron pairing of the 1uc-FeSe/STO system, especially with the EPHC and EPLC treated on equal footing. We first show within a generalized Eliashberg formalism that the EPHC alone can only yield a low T_c of a few Kelvin. However, there exists a distinct regime in which the EPHC and EPLC mechanisms, both inherently connected to the ions, can naturally join force in enhancing the T_c by one order of magnitude to the experimentally observed range [8–10]. Remarkably, such a cooperative effect is not operative in good metals with high-energy plasmons. The underlying microscopic mechanism is attributed to the substantially weakened Coulomb pseudopotential in the presence of the low energy plasmon excitations. In sharp contrast, such a weakening effect cannot be expected within a simple “phonon + phonon” picture of two phononic modes. The present “phonon + plasmon” mechanism also embodies characteristic dependences of T_c on the carrier density and

*Corresponding author: zhangzy@ustc.edu.cn

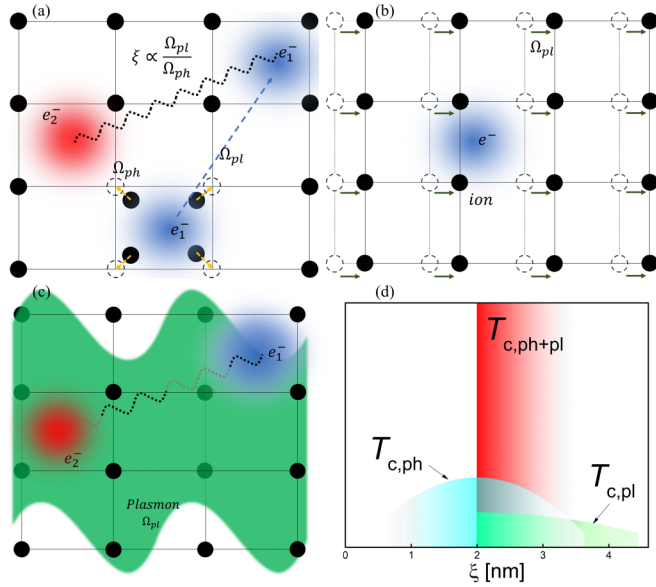


FIG. 1. (a) Schematic of the electron pairing mediated by the EPHC. (b) Schematic of the optical plasmon mode from the perspective of electrons. The arrows indicate the displacements of the ionic cores. (c) Schematic of the electron pairing mediated by the EPLC. The green waves represent the plasmonic oscillations of the conduction electrons, and the wavy lines connecting two electrons in (a) and (c) indicates their pairing. (d) Distributions of the coherence lengths (ξ) due to the EPHC (blue area) and EPLC (green area) mechanisms, with the overlapping and strongly constructive region of the two highlighted in red as defined above the threshold of the EPLC coherence length. Quantitative determinations of ξ are to be presented in Sec. IV.

isotope substitution, and may find broad applicability in many superconducting systems with low carrier densities, including, most notably, the cuprates.

II. EPHC AND EPLC ON EQUAL FOOTING

Before specifying to the concrete system of 1uc-FeSe/STO, we first elucidate the close analogy and generality of the EPHC and EPLC mechanisms in mediating electron pairing. As illustrated in Fig. 1(a), the well-established EPHC mechanism is rooted in the attraction felt by one electron due to the lattice distortion (or vibration) induced by another electron. The plasmon mediated electron pairing is less well accepted, but on a principle level is universally present as well, as illustrated in Figs. 1(b) and 1(c). Physically, the plasmon mode is the collective oscillations of the conduction electrons against the static positive ionic lattice that provides the restoring force. From the view point of the electrons, the plasmon mode can be equivalently viewed as the collective oscillations of the lattice, as schematically shown in Fig. 1(b), which also underscores the optical nature of the plasmon. The EPLC mechanism is rooted in the attractive force of two electrons mediated by the plasmonic mode or equivalently the collective oscillations of the lattice [see Fig. 1(c)] [37]. Here, it is worthwhile to emphasize that the dynamic lattice nature of the EPHC and static lattice nature of the EPLC are conceptually independent, each tied to its own physics origin.

Furthermore, the very fact that both mechanisms are naturally rooted in lattice strongly implies that the two can also work constructively in mediating electron pairing, especially when the collective modes involved are comparable in energy, as in the 1uc-FeSe/STO system. In contrast, such inherent superiority is absent in those previously proposed “phonon + spin fluctuation” picture.

Besides the two pairing glues discussed above, another vitally important character is the overlapping coherence lengths of the Cooper pairs due to the EPHC and EPLC mechanisms. Within the standard BCS picture, the average coherence length mediated by the EPHC is much larger than the lattice constant as a result of the strong adiabatic effect depicted in Fig. 1(a) [23,24]. Here, electron e_1 distorts the lattice, then moves away with the plasmon frequency Ω_{pl} . If electron e_2 reaches the distorted region before the lattice relaxes to its equilibrium configuration, e_1 and e_2 can pair via indirect interaction through the lattice. Correspondingly, the EPHC-mediated coherence length is proportional to Ω_{pl}/Ω_{ph} , which is on the order of tens of nanometers for conventional superconductors. But for the systems with low carrier densities, like the 1uc-FeSe/STO, due to the strong nonadiabatic nature of the EPHC as manifested in the form of dynamic polarons, the coherence length is only on the order of 1 nm [18]. In contrast, given the long-range nature of the EPLC, the corresponding coherence length has a lower bound determined by the wave vector of the highest Ω_{pl} . For the EPHC and EPLC mechanisms to work constructively rather than each working independently on its own, one necessary condition is the existence of an overlapping range between the EPHC and EPLC coherence lengths, as shown in Fig. 1(d), and also quantitatively substantiated in later presentations for 1uc-FeSe/STO.

The general Hamiltonian containing both the EPHC and EPLC can be expressed as

$$H = H_0 + H_{ep} + H_{ee}, \quad (1)$$

$$H_0 = \sum_{p\sigma} \xi_p C_{p\sigma}^+ C_{p\sigma} + \Omega_{ph} \sum_q A_q^+ A_q + \Omega_{pl} \sum_q B_q^+ B_q, \quad (2)$$

$$H_{e-p} = \frac{1}{\sqrt{v}} \left(\sum_{pq\sigma} g_q^{ph} C_{p+q\sigma}^+ C_{p\sigma} A_q^+ + \sum_{pq\sigma} g_q^{pl} C_{p+q\sigma}^+ C_{p\sigma} B_q^+ \right), \quad (3)$$

$$H_{e-e} = \frac{1}{2v} \sum_{pp'q\sigma} v_q C_{p+q,\sigma}^+ C_{p'-q,\sigma}^+ C_{p\sigma} C_{p',\sigma}. \quad (4)$$

Here, H_0 is the noninteracting Hamiltonian for electron, phonon and plasmon, ξ_p is the electron dispersion, C_p^+ , A_q^+ , and B_q^+ (C_p , A_q , and B_q) are the corresponding creation (annihilation) operators. For the specific 1uc-FeSe/STO system, we take the highest α -phonon mode with frequency $\Omega_{ph} \sim 97$ meV from experiment [18,25]. The plasmon frequency Ω_{pl} will be specified later, whose value has also been cross checked by experimental measurement. In doing so, the EPHC and EPLC are inherently coupled, and the polaronic plasmon nature is fully considered within our picture. H_{e-p} is the interaction containing both the EPHC and EPLC, with g_q^{ph} and g_q^{pl} the corresponding coupling matrix elements. H_{e-e}

is the electron-electron (e-e) interaction, with $v_q = 4\pi e^2/q^2$ describing the bare three-dimensional (3D) Coulomb repulsion, and the 3D nature is signified by the optical nature of the plasmon mode observed experimentally [18]. Here, to highlight the role of the EPLC, we have treated it separately from the remaining e-e interaction, and the double counting will be explicitly avoided, and discussed later.

Based on the above discussions and the observed *s*-wave superconducting gap from experiments [9,44], we now treat the EPHC and EPLC equally by generalizing the isotropic Eliashberg equations [45,46] as

$$Z(i\omega_n) = 1 + \frac{\pi T}{\omega_n} \sum_{n'} \frac{\omega_{n'}}{\sqrt{\omega_{n'}^2 + \Delta(i\omega_{n'})^2}} \lambda_{\text{tot}}(i\omega_n - i\omega_{n'}), \quad (5)$$

$$Z(i\omega_n) \Delta(i\omega_n) = \pi T \sum_{n'} \frac{\Delta(i\omega_{n'})}{\sqrt{\omega_{n'}^2 + \Delta(i\omega_{n'})^2}} K(i\omega_n - i\omega_{n'}) \quad (6)$$

$$K(i\omega_n - i\omega_{n'}) = \mu^*(i\omega_n - i\omega_{n'}) - \lambda_{\text{tot}}(i\omega_n - i\omega_{n'}). \quad (7)$$

Here, $i\omega_n$ and $i\omega_{n'}$ are the Matsubara frequencies of the electrons, $Z(i\omega)$ is the electron mass renormalization function, $\Delta(i\omega)$ is the superconducting gap function, $\mu^*(i\omega)$ is the reduced frequency-dependent Coulomb repulsion, and $\lambda_{\text{tot}}(i\omega)$ is an auxiliary function describing the total electron-boson coupling. Here, in discussing the e-e attraction mediated by electron-boson coupling, the plasmon and phonon modes can be treated on equal footing, which results in the expression shown in Eq. (8) below when both bosonic modes are represented by their respective Einstein modes:

$$\lambda_{\text{tot}}(i\omega) = \frac{\lambda_{\text{ph}} * \Omega_{\text{ph}}^2}{\omega^2 + \Omega_{\text{ph}}^2} + \frac{\lambda_{\text{pl}} * \Omega_{\text{pl}}^2}{\omega^2 + \Omega_{\text{pl}}^2}, \quad (8)$$

where λ_{ph} and λ_{pl} are the corresponding coupling strengths, respectively. It is necessary to emphasize that the validity of Eq. (8), namely, the consequent constructive interplay between EPHC and EPLC, is based on their overlapped coherence lengths in Fig. 1(d).

Before proceeding any further, we first justify the validity of the Eliashberg formalism adopted here. Based on Migdal's theorem [47], the Eliashberg formalism would break down in nonadiabatic regime ($\Omega_{\text{ph}} \sim E_F$), because this formalism has neglected vertex corrections in the many-body interaction, while such vertex corrections measured by $\lambda\Omega_{\text{ph}}/E_F$ cannot be readily neglected for reasonable strengths of λ . Nevertheless, the vertex corrections beyond the Eliashberg formalism can still be small enough to be perturbatively treated as long as λ is small [26,32,48]. In doing so, as demonstrated in Ref. [48], T_c can be significantly enhanced only within the forward-scattering approximation, and stays nearly as a constant when all the scattering processes are included. When specified to the present system of 1uc-FeSe/STO, the electron-boson coupling strengths are relatively small (see detailed calculations later), and the backward scattering channels are as important as the forward scattering ones [18]. Accordingly, the T_c enhancement from the vertex corrections becomes negligibly small and the Eliashberg formalism adopted here can provide a reasonably reliable description of T_c for the nonadiabatic 1uc-FeSe/STO system.

Beyond the considerations of the finite momenta of the bosonic modes, we also note that for 1uc-FeSe/STO, the observed Fermi surface is distinctly isotropic [9,10,16], and the system exhibits an *s*-wave superconducting gap [9,44]. Therefore it is justified to neglect the electronic momentum dependence in the Eliashberg formalism [48], aside from a specific account of the magnitude of the Fermi wave vector. On the other hand, in the present study, we find the frequency dependence (namely, the dynamic nature) plays a dominant role in enhancing the T_c , which is the central message to be conveyed.

III. EPLC WEAKENED COULOMB PSEUDOPOTENTIAL

In the following, we elucidate the different aspects of the dynamical nature of the reduced Coulomb repulsion $\mu^*(i\omega)$ in Eq. (7). In conventional superconductors, $\mu^*(i\omega)$ is commonly approximated as an instantaneous constant, because the energy scale of Ω_{pl} is too large to be relevant to the superconductivity [23,24]. For systems with relatively low Ω_{pl} , its dynamical nature is nonnegligible and care must be taken when the EPLC and reduced dynamical Coulomb repulsion are both considered explicitly, to avoid double counting. This can be achieved by separating the EPLC from the total dynamical *e-e* interaction as follows, similar to the separation of the EPHC from the total *e-e* interaction established previously [49].

We first identify the EPLC contribution in the screened *e-e* interaction $\mu(i\omega)$ expressed as

$$\mu(i\omega) = \frac{1}{4\pi^2 v_F} \int_0^{2k_F} \frac{qv_q}{\epsilon(q, i\omega)} dq. \quad (9)$$

Here, v_F is the Fermi velocity, k_F is the Fermi wave vector, and $\epsilon(q, i\omega)$ is the frequency-dependent dielectric function. It is worth to note that the range of the momentum integration $2k_F$ encompasses all the electron-boson scattering processes (namely, through both EPHC and EPLC) within the parabolic band of focus. Within the random phase approximation (RPA), $\epsilon(q, i\omega)$ is given as

$$\epsilon(q, i\omega) = \epsilon_\infty - \frac{v_q}{N} \sum_{\mathbf{p}, \sigma} \frac{n_F(\xi_{\mathbf{p}}) - n_F(\xi_{\mathbf{p}+\mathbf{q}})}{\xi_{\mathbf{p}} - \xi_{\mathbf{p}+\mathbf{q}} + i\omega}, \quad (10)$$

where ϵ_∞ is the optical dielectric constant, $\xi_{\mathbf{p}}$ and $\xi_{\mathbf{p}+\mathbf{q}}$ are the respective electron and hole energies measured from the Fermi level, N is the electron density of states at the Fermi level, and n_F is the Fermi distribution function. For the 1uc-FeSe/STO system, we plot $\epsilon(q, i\omega)$ on the imaginary frequency axis in Fig. 2(a) by only considering the contributions of the bands cross the Fermi level, which are essentially degenerate [16]. Our adopted band dispersion for the 1uc-FeSe/STO system is fitted from the experimental observations in Fig. 2(a) of Ref. [18], which is parabolic, with an effective electron mass $m^* = 2.9m_e$. Here, the two black dashed lines represent the optical and acoustic plasmons defined by $\epsilon(q, i\omega) = 0$. The long wavelength limit of Ω_{pl} is ~ 160 meV, which agrees with the experimentally measured value [18]. In our calculations, we have set $\epsilon_\infty = 10$, close to the value for Nb-doped SrTiO₃ [50].

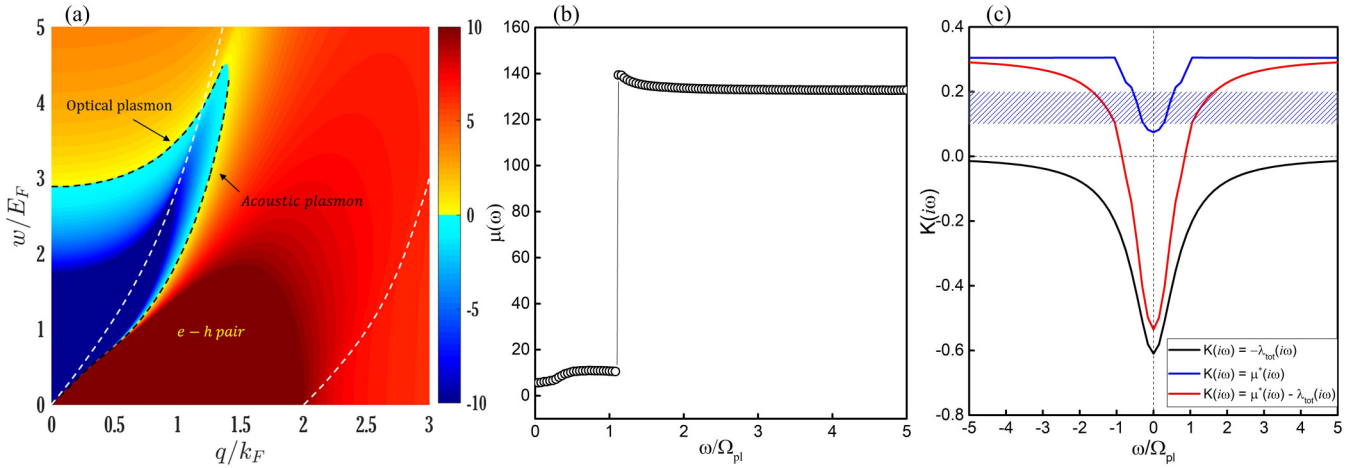


FIG. 2. (a) Dielectric function $\epsilon(q, i\omega)$ calculated within the RPA for 1uc-FeSe/STO, with the blue region highlighting the regime with $e-e$ attraction. The optical nature of the plasmon mode is tied to the 3D nature of the interfacial electrons in the system. The Fermi energy of $E_F = 56$ meV is adopted from Ref. [18]. (b) Frequency dependence of the screened Coulomb repulsion $\mu(i\omega)$ as obtained from Eq. (9) with $\epsilon(q, i\omega) > 0$. (c) Dynamical structures of the boson-mediated attraction $\lambda_{\text{tot}}(i\omega)$, the Coulomb pseudopotential $\mu^*(i\omega)$, and the total $e-e$ interaction $K(i\omega) = \mu^*(i\omega) - \lambda_{\text{tot}}(i\omega)$ on the imaginary frequency axis. The shaded region represents the typical range of the instantaneous Coulomb pseudopotential in conventional superconducting systems. The Coulomb pseudopotential here is directly calculated from Eq. (21).

The dielectric function between the optical and acoustic plasmons is negative, signifying the attractive $e-e$ interaction induced by the EPLC. These results provide the basis that the EPLC could effectively reduce the Coulomb repulsion, and even further induce electron pairing in the regime of low carrier density, thereby potentially sustaining superconductivity without the EPHC [51]. We also note that the EPLC mediated attraction might be overestimated within the RPA [52]. To avoid this problem, we separate the EPLC mediated attraction from the repulsive part of the dynamical $e-e$ interaction in Eq. (9) as follows [49]:

$$\mu(i\omega) = \frac{1}{4\pi^2 v_F} \int_0^{2k_F} \frac{q v_q}{\epsilon_+(q, i\omega)} dq - V_{\text{EPLC}}, \quad (11)$$

with $\epsilon_+(q, i\omega)$ indicating only the positive part of the dielectric function and treated within the RPA in Eq. (10), while the attractive EPLC part is absorbed into Eq. (8) on equal footing with the EPHC, with $\lambda_{\text{pl}} = 0.25$ estimated from Appendix A. The accuracy of the RPA in estimating the screened Coulomb repulsion is confirmed through our explicit calculations of the plasmon frequency for the 1uc-FeSe/STO system, yielding Ω_{pl} that is consistent with the experimental observations [18]. Detailed numerical calculations of the first term in Eq. (11) further give the steplike Coulomb repulsion shown in Fig. 2(b).

In Fig. 2(b), we show the calculated screened $e-e$ repulsion $\mu(i\omega)$ of 1uc-FeSe/STO as depicted in the first term of Eq. (11). In deriving the steplike behavior in Fig. 2(b), we have explicitly treated the dispersive nature of the dominant plasmon mode contained in the dielectric function $\epsilon(q, i\omega)$, as marked by the black dashed line in Fig. 2(a). Physically, the Coulomb repulsion is largely screened at frequencies smaller than Ω_{pl} , while less screened at frequencies larger than Ω_{pl} . Qualitatively, the frequency dependence of the Coulomb repulsion could be divided into two parts according to Ω_{pl} in Fig. 2(b), and is less dispersive on either side. For the feasibility of obtaining analytical integrations, we replace this complex curve of $\mu(i\omega)$ by a step function as follows:

$$\mu(i\omega) = \begin{cases} \mu_1, & (\omega < \Omega_{\text{pl}}) \\ \mu_2, & (\omega > \Omega_{\text{pl}}) \end{cases}, \quad (12)$$

where μ_1 and μ_2 are constants representing the values for the screened $e-e$ repulsion with frequency smaller or larger than Ω_{pl} , respectively.

Now, we move to the Coulomb pseudopotential by solving the self-consistent gap equations [24], while maintaining the frequency-dependent screened $e-e$ interaction as

$$\Sigma'_1(\omega) = \Delta_0[(1 + \xi)U(\omega) - \xi], \quad (13)$$

$$\begin{aligned} \Sigma'_2(\omega) = & \Delta_0 \int_0^{\Delta_0} \frac{[(1 + \xi)U(z) - \xi][\lambda U(\omega - z) - \mu(\omega - z)]}{i(\Delta_0^2 - z^2)^{1/2}} dz, \\ & + \Delta_0 \int_{\Delta_0}^{\Omega_{\text{cut}}} \frac{[(1 + \xi)U(z) - \xi][\lambda U(\omega - z) - \mu(\omega - z)]}{(z^2 - \Delta_0^2)^{1/2}} dz, \end{aligned} \quad (14)$$

where Δ_0 corresponds to the superconducting gap and ξ is the auxiliary parameter in introducing the trial function, λ is the joint electron-boson coupling strength, and Ω_{cut} is the truncation energy of electrons. $\Sigma'_1(\omega)$ is the trial gap function, and $\Sigma'_2(\omega)$ is the gap function to be calculated self-consistently. Within the Einstein mode approximation, the phonon Green's function

is defined as $U(\omega) = \frac{\omega_q^2}{\omega_q^2 - \omega^2}$. As pointed out previously [24], the integration can only be done analytically in the limit where the frequency is much smaller or much larger than Ω_{ph} due to the singularity in $U(\omega)$ at $\omega = \Omega_{\text{ph}}$ [24]. Consequently, Ω_{ph} and Ω_{pl} can be approximately viewed equally in these two limits, and the EPLC contribution is contained in the electron-boson coupling strength λ . Here, the EPLC associated with the bosonic plasmon mode can be treated on equal footing with the EPHC in mediating e-e attraction, justifying the validity of Eq. (14).

The integrations in Eq. (14) are carried out analytically, and the obtained gap equations are

$$\Sigma'_2(\omega) \approx \Delta_0 \left[\lambda \ln \left(\frac{2\Omega_{\text{ph}}}{\Delta_0} \right) - \mu_1 \ln \left(\frac{2\Omega_{\text{ph}}}{\Delta_0} \right) + \mu_2 \xi \ln \left(\frac{\Omega_{\text{cut}}}{\Omega_{\text{ph}}} \right) \right], \quad \omega \ll \Omega_{\text{ph}}, \quad (15)$$

$$\Sigma'_2(\omega) \approx -\Delta_0 \left[\mu_1 \ln \left(\frac{2\Omega_{\text{ph}}}{\Delta_0} \right) - \mu_2 \xi \ln \left(\frac{\Omega_{\text{cut}}}{\Omega_{\text{ph}}} \right) \right], \quad \omega \gg \Omega_{\text{ph}}, \quad (16)$$

where only the real part of the obtained gap function is shown. When comparing the obtained $\Sigma'_2(\omega)$ in Eqs. (15) and (16) with the limiting cases of the trial function $\Sigma'_1(\omega)$ in Eq. (13), the parameters Δ_0 and ξ need to satisfy the following two conditions:

$$(\lambda - \mu_1) \ln \left(\frac{2\Omega_{\text{ph}}}{\Delta_0} \right) + \mu_2 \xi \ln \left(\frac{\Omega_{\text{cut}}}{\Omega_{\text{ph}}} \right) = 1, \quad (17)$$

$$\mu_1 \ln \left(\frac{2\Omega_{\text{ph}}}{\Delta_0} \right) - \mu_2 \xi \ln \left(\frac{\Omega_{\text{cut}}}{\Omega_{\text{ph}}} \right) = \xi. \quad (18)$$

Solving the above two equations, we obtain the superconducting gap as follows:

$$\ln \left(\frac{2\Omega_{\text{ph}}}{\Delta_0} \right) = \left[\lambda - \frac{\mu_1}{1 + \mu_2 \ln \left(\frac{\Omega_{\text{cut}}}{\Omega_{\text{ph}}} \right)} \right]^{-1}. \quad (19)$$

The obtained Coulomb pseudopotential μ^* with the frequency dependent Coulomb repulsion retained is

$$\mu^* = \frac{\mu_1}{1 + \mu_2 \ln \left(\frac{\Omega_{\text{cut}}}{\Omega_{\text{ph}}} \right)}. \quad (20)$$

Here, the Coulomb pseudopotential is largely suppressed due to the strong Coulomb repulsion μ_2 at high frequencies [see Fig. 2(b)], and it restores to the traditional form $\mu^* = \mu / (1 + \mu \ln(\Omega_{\text{cut}} / \Omega_{\text{ph}}))$ in the static regime with $\mu_1 = \mu_2$. Here, it is worth to note that we can reproduce this simple but important relation later in Eq. (30), using a much simpler trial function, indicating its correctness and robustness rooted in the underlying physics and irrespective of the trial functions.

We notice that the obtained Coulomb pseudopotential in Eq. (20) is of the static form that does not capture its dynamic nature, which is proven to be important for superconductivity in previous studies [38,53]. A rigorous analytical derivation of its full frequency-dependent form is presently beyond reach. Instead, we take an *ad hoc* generalization to other frequencies as follows:

$$\mu^*(\omega) = \begin{cases} \frac{\mu(\omega)}{1 + \mu(\Omega_{\text{cut}}) \ln \left(\frac{\Omega_{\text{pl}}}{\Omega_{\text{ph}}} \right)}, & \omega < \Omega_{\text{pl}} \\ \frac{\mu(\omega)}{1 + \mu(\omega) \ln \left(\frac{\Omega_{\text{cut}}}{\Omega_{\text{ph}}} \right)}, & \omega > \Omega_{\text{pl}} \end{cases}. \quad (21)$$

Here, the generalized frequency-dependent Coulomb pseudopotential is based on physical intuitions, in that it properly reduces to the expected limiting qualitative behaviors for higher or lower frequencies. Qualitatively, these findings agree well with the recently reported dynamical Coulomb

repulsion structure of the superconductivity in lithium using a first-principles approach [38]. We have also tested the convergence of T_c on the truncation frequency Ω_{cut} in Appendix B, which gives $\Omega_{\text{cut}} \sim 15\Omega_{\text{pl}}$. We should emphasize that we intentionally choose a relatively smaller cutoff energy of $\Omega_{\text{cut}} = 15\Omega_{\text{pl}}$ in the dynamical case, which may overestimate the T_c by at most a few Kelvin in Fig. 4(c). Such an accuracy is acceptable within the scope of present study. In doing so, we also avoid the likely scenario of invoking ill-defined quasiparticles when a too large cutoff energy is taken [43].

In Fig. 2(c), we illustrate the different interaction kernels $K(i\omega)$ on the imaginary frequency axis, including the total electron-boson coupling $\lambda_{\text{tot}}(i\omega)$, the Coulomb pseudopotential $\mu^*(i\omega)$, and the effective e-e interaction $\mu^*(i\omega) - \lambda_{\text{tot}}(i\omega)$ for 1uc-FeSe/STO at optimal doping, where the electron energy dispersions are fitted from experimental observations [10]. Here, we choose a modest EPHC strength $\lambda_{\text{ph}} \sim 0.36$ within the range (0.2–0.5) given from theoretical and experimental considerations [16,24,54–56], and the EPLC strength is calculated to be $\lambda_{\text{pl}} \sim 0.25$ (see Appendix A). Here again, both couplings are relatively weak, which guarantees the validity of the Eliashberg equations. As a comparison, we also plot as the blue shaded region the instantaneous Coulomb pseudopotential $\mu^* = 0.1\text{--}0.2$ typically adopted in conventional superconductors [57], which would severely underestimate the Coulomb repulsion at high frequencies.

IV. ENHANCED T_c FROM THE COOPERATIVE EFFECT OF EPHC AND EPLC

Next, we shift our focus to the superconducting transition temperature T_c for 1uc-FeSe/STO at optimal doping due to the EPHC or jointly with EPLC, within the generalized Eliashberg formalism. In Fig. 3(a), we first show the temperature dependence of the superconducting gap at the Fermi level due to the EPHC alone, with the Coulomb pseudopotential taking its static limit of $\mu^*(i\omega) = \mu^*(0) \sim 0.076$ in Fig. 2(c). The resulting $T_{c,\text{ph}} \sim 6$ K. Clearly, the EPHC alone is insufficient to explain the high T_c observed at optimal doping of the 1uc-FeSe/STO. We note that our phonon-only results are quantitatively consistent with that of an existing related study [56]. Furthermore, in several recent studies [26,32,58], high T_c 's were predicted within a modified BCS framework invoking forward electron-phonon scattering [16], a picture that is still under active debate [18,29].

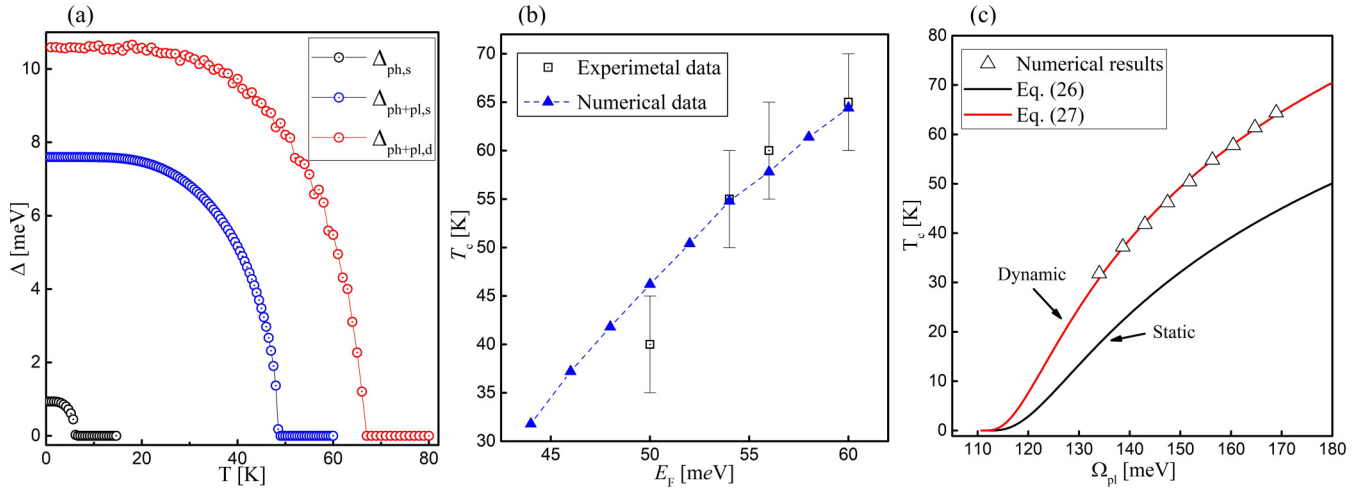


FIG. 3. (a) Evolution of the superconducting gap with temperature within different mechanisms. (b) Evolution of T_c at increasing interfacial carrier density as measured by the Fermi energy. Here, our calculated results (blue solid triangles) are compared with available experimental data (empty squares) [10]. (c) Evolution of T_c at increasing interfacial carrier density as measured by the plasmon frequency. Here, the data (empty triangles), black, and red curves are from our numerical results, Eqs. (31) and (32), respectively.

Now, we consider the constructive interplay of the EPHC and EPLC mechanisms based on the overlapped coherence lengths. The EPLC is of long range in nature, and the corresponding coherence length has a lower bound defined by the largest momentum of the plasmon mode, given by $\xi_{pl} \sim 2\pi/q_{max} \sim 2$ nm with $q_{max} \sim 1.3 k_F$ [see Fig. 2(a)] and $k_F \sim 0.22 \text{ \AA}^{-1}$ [9,10]. Separately, the average coherence length mediated by the EPHC is decided by the ratio $\Omega_{pl}(q_{max})/\Omega_{ph} \sim 2.5$ in 1ucFeSe/STO, yielding $\xi_{ph} \sim 2$ nm [18]. Therefore, constructive interplay between the EPHC and EPLC is expected in the range around 2 nm [see in Fig. 1(d)], and

encouragingly, this range is also consistent with the pairing sizes observed experimentally [8,44].

We then obtain the constructive interplay of the EPHC and EPLC on T_c , with the Coulomb pseudopotential first treated in the static limit. The corresponding temperature evolution of $\Delta_{ph+pl,s}$ is shown in Fig. 3(a), and the resultant $T_{c,s} \sim 50$ K is far beyond $T_{c,ph}$ obtained earlier. The strikingly large enhancement in T_c can be rationalized from three aspects, one transparent, the other two more subtle. Obviously, the total attractive strength of electron pairing is naturally strengthened by the joint efforts of both the phonon and plasmon modes as bosonic glues, as each glue only needs to overcome a fraction of the total Coulomb repulsion. At a more subtle level, the formation of plasmon itself necessarily consumes the static long-range part of the Coulomb repulsion [59,60]. Furthermore, the dynamic nature of the EPLC further renormalizes the Coulomb repulsion, resulting in a substantially weakened Coulomb pseudopotential due to the cooperative effects of retardation and renormalization [see Eqs. (20) and (21)]. Beyond these three factors, the large enhancement also stems from the nonlinear dependence of T_c on the total pairing strength [see Eq. (32)].

Next, we assess the role of the dynamical structure of the Coulomb pseudopotential in electron pairing, expected to be particularly important for 1uc-FeSe/STO with low carrier densities. The results are shown in Fig. 3(a). Indeed, the resultant $T_{c,d}$ due to the interplay between the EPHC and EPLC is further enhanced in the dynamic regime from $T_{c,s}$ of the static regime, reaching ~ 67 K, and falling into the experimentally observed range [8–10,14]. At a more subtle level, the effect of the dynamical Coulomb pseudopotential is mainly manifested by the dynamical electron correlations in the frequency space [53], as elaborated in more detail in Appendix B. It is also worth to caution on the absolute magnitudes of the difference between static and dynamic T_c 's, which can be enlarged by the choices of the cutoff energies in Figs. 4(a) and 4(c). On the other hand, even with much larger cutoff energies, the dynamic T_c is still substantially higher than the static T_c ,

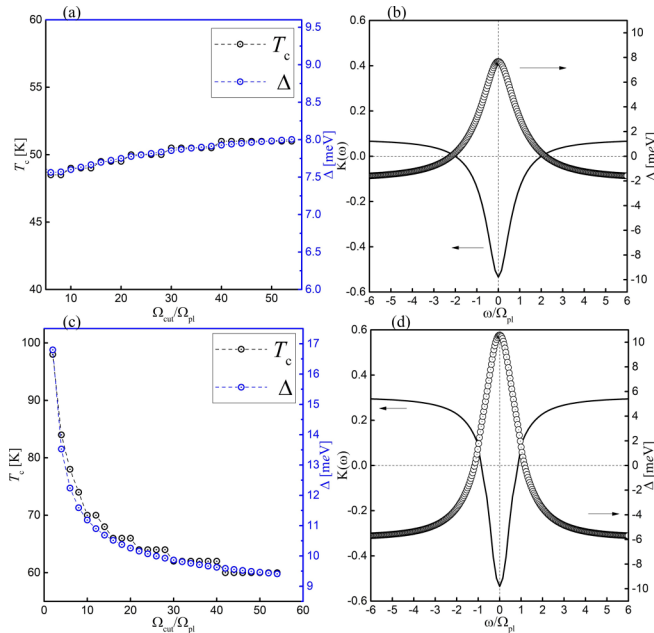


FIG. 4. (a) T_c evolution with Ω_{cut} in the static limit of the Coulomb pseudopotential. (b) The corresponding gap function at $T = 2.5$ K and the total e-e interaction on the imaginary frequency axis. (c) and (d), same as (a) and (b), but in the dynamical regime.

reaffirming the validity of dynamically enhanced superconductivity at the qualitative level.

V. CHARACTERISTIC DEPENDENCIES OF T_c

We finally examine the characteristic dependencies of T_c on various controllable physical parameters, including the interfacial electron density and isotope substitution. For the 1uc-FeSe/STO system, given that the electronic screening effect is much weaker in the direction perpendicular to the FeSe plane, the EPHC should exhibit only weak dependence

on the electron doping. In contrast, the plasmon related parameters should naturally depend on the electron doping in a more sensitive manner. In Fig. 3(b), we plot the calculated T_c evolution with the Fermi energy, together with several experimentally observed values [10], displaying quantitative agreements. Beyond such numerical results, we can also obtain a characteristic dependence of T_c on Ω_{pl} .

To derive the analytic expression of T_c based on the picture presented above, we start with the following pairing equation at the transition temperature T_c , with the EPHC, the EPLC, and frequency-dependent Coulomb repulsion considered explicitly:

$$\Delta(\omega) = \frac{1}{Z(\omega)} \left\{ \int_0^\infty \frac{d\omega'}{\omega'} \text{Re} [\Delta(\omega')] [H_{\text{ph}}(\omega') + H_{\text{pl}}(\omega')] - \int_0^\infty \frac{d\omega'}{\omega'} \mu(\omega - \omega') \text{Re} [\Delta(\omega')] [1 - 2f(\omega')] \right\}, \quad (22)$$

$$H_{\text{ph(pl)}}(\omega') = \int_0^{\Omega_{\text{ph(pl)}}} d\omega_q \alpha_{\text{ph(pl)}}^2(\omega_q) F_{\text{ph(pl)}}(\omega_q) \{ [N(\omega_q) + f(-\omega')] [(\omega' + \omega_q + \omega)^{-1} + (\omega' + \omega_q - \omega)^{-1}] - [N(\omega_q) + f(\omega')] [(-\omega' + \omega_q + \omega)^{-1} + (-\omega' + \omega_q - \omega)^{-1}] \}. \quad (23)$$

Here, ω and ω_q are the electron and boson (phonon or plasmon) energies, $\Delta(\omega)$ is the superconducting gap function, $\alpha_{\text{ph(pl)}}(\omega)$ is the electron-phonon or electron-plasmon coupling strength, $F_{\text{ph(pl)}}(\omega)$ is the boson density of states function, and $N(\omega_q)$ and $f(\omega)$ are the boson and electron distribution function, respectively. The frequency-dependent screened Coulomb repulsion $\mu(\omega)$ has been simplified as in Eq. (12). An approximate solution to Eq. (22) can be obtained by substituting a trial function for $\Delta(\omega)$ and then performing the integration self-consistently. The trial $\Delta'(\omega)$ can be chosen as [57]

$$\Delta'(\omega) = \begin{cases} \Delta_0, & 0 < \omega < \Omega_{\text{pl}}, \\ \Delta_\infty, & \omega > \Omega_{\text{pl}} \end{cases}, \quad (24)$$

and $\Delta(0)$ and $\Delta(\infty)$ can be calculated from Eq. (22) as follows:

$$\Delta(0) = \frac{1}{Z(0)} \left\{ \Delta_0 \left[\lambda_{\text{ph}} \ln \left(\frac{\Omega_{\text{ph}}}{T_c} \right) + \lambda_{\text{pl}} \ln \left(\frac{\Omega_{\text{pl}}}{T_c} \right) - \mu_1 \ln \left(\frac{\Omega_{\text{pl}}}{T_c} \right) \right] + \Delta_\infty \left[\frac{\lambda_{\text{ph}} \langle \omega_{\text{ph}} \rangle}{\Omega_{\text{ph}}} + \frac{\lambda_{\text{pl}} \langle \omega_{\text{pl}} \rangle}{\Omega_{\text{pl}}} - \mu_2 \ln \left(\frac{\Omega_{\text{cut}}}{\Omega_{\text{pl}}} \right) \right] \right\}, \quad (25)$$

$$\Delta(\infty) = -\frac{1}{Z(\infty)} \left[\mu_1 \Delta_0 \ln \left(\frac{\Omega_{\text{pl}}}{T_c} \right) + \mu_2 \Delta_\infty \ln \left(\frac{\Omega_{\text{cut}}}{\Omega_{\text{pl}}} \right) \right], \quad (26)$$

where Ω_{cut} is adopted to truncate the electron energy in the second integration in Eq. (22). The averaged bosonic frequencies $\langle \omega_{\text{ph(pl)}} \rangle$ is expressed by

$$\langle \omega_{\text{ph(pl)}} \rangle = \frac{\int_0^{\Omega_{\text{ph(pl)}}} d\omega_q \alpha_{\text{ph(pl)}}^2(\omega_q) F_{\text{ph(pl)}}^2(\omega_q)}{\int_0^{\Omega_{\text{ph(pl)}}} \frac{d\omega_q}{\omega_q} \alpha_{\text{ph(pl)}}^2(\omega_q) F_{\text{ph(pl)}}^2(\omega_q)}. \quad (27)$$

When we consider only the highest phonon mode and the optical plasmon mode within the Einstein mode approximation, we have $\langle \omega_{\text{ph(pl)}} \rangle = \Omega_{\text{ph(pl)}}$. The renormalization is found to be $Z(\infty) = 1$ and $Z(0) = 1 + \lambda_{\text{tot}} = 1 + \lambda_{\text{ph}} + \lambda_{\text{pl}}$. In Eqs. (25) and (26), we have also defined $\lambda_{\text{ph(pl)}}$ as

$$\lambda_{\text{ph(pl)}} = 2 \int_0^{\Omega_{\text{ph(pl)}}} \frac{d\omega_q}{\omega_q} \alpha_{\text{ph(pl)}}^2(\omega_q) F_{\text{ph(pl)}}^2(\omega_q). \quad (28)$$

Next, self-consistency requires $\Delta(0) = \Delta_0$ and $\Delta(\infty) = \Delta_\infty$. Then we have

$$\Delta(0) = \Delta_0 = \frac{1}{1 + \lambda_{\text{tot}}} \left\{ \Delta_0 \left[\lambda_{\text{ph}} \ln \left(\frac{\Omega_{\text{ph}}}{T_c} \right) + \lambda_{\text{pl}} \ln \left(\frac{\Omega_{\text{pl}}}{T_c} \right) - \mu_1 \ln \left(\frac{\Omega_{\text{pl}}}{T_c} \right) \right] + \Delta_\infty \left[\lambda_{\text{tot}} - \mu_2 \ln \left(\frac{\Omega_{\text{cut}}}{\Omega_{\text{pl}}} \right) \right] \right\}, \quad (29)$$

$$\Delta(\infty) = \Delta_\infty = -\mu_1 \Delta_0 \ln \left(\frac{\Omega_{\text{pl}}}{T_c} \right) - \mu_2 \Delta_\infty \ln \left(\frac{\Omega_{\text{cut}}}{\Omega_{\text{pl}}} \right) = -\frac{\mu_1 \Delta_0 \ln \left(\frac{\Omega_{\text{pl}}}{T_c} \right)}{1 + \mu_2 \ln \left(\frac{\Omega_{\text{cut}}}{\Omega_{\text{pl}}} \right)} \quad (30)$$

$$= -\mu^* \Delta_0 \ln \left(\frac{\Omega_{\text{pl}}}{T_c} \right),$$

where $\mu^* = \mu_1 / (1 + \mu_2 \ln(\Omega_{\text{cut}}/\Omega_{\text{pl}}))$ is the Coulomb pseudopotential, which has the same form as Eq. (20).

Solving Eqs. (29) and (30) together, we have

$$T_c = \Omega_{\text{ph}} \left(\frac{\Omega_{\text{ph}}}{\Omega_{\text{pl}}} \right)^{\frac{\lambda_{\text{pl}} - \mu^*(1 + \lambda_{\text{tot}})}{\lambda_{\text{tot}} - \mu^*(1 + \lambda_{\text{tot}})}} \exp \left[-\frac{\lambda_{\text{tot}} + 1}{\lambda_{\text{tot}} - \mu^*(\lambda_{\text{tot}} + 1)} \right] (\text{static}), \quad (31)$$

$$T_c = \frac{\Omega_{\text{ph}}}{1.571} \left(\frac{\Omega_{\text{pl}}}{\Omega_{\text{ph}}} \right)^{\frac{\lambda_{\text{pl}} - \mu^*(\lambda_{\text{tot}} + 1)}{\lambda_{\text{tot}} - \mu^*(\lambda_{\text{tot}} + 1)}} \exp \left[-0.758 \frac{\lambda_{\text{tot}} + 1}{\lambda_{\text{tot}} - \mu^*(\lambda_{\text{tot}} + 1)} \right] (\text{dynamic}). \quad (32)$$

In the above derivation of T_c , the dynamic electron correlation effect has not been included, as reflected by the static form μ^* . With the inclusion of the dynamical electron correlation effect, a mathematically rigorous form cannot be obtained, but the numerical results can still be well fitted by Eq. (32) above. The two system-dependent fractional constants appearing in Eq. (32) are determined by fitting the numerical results shown in Fig. 3(c), to capture the effect from the dynamical nature of the Coulomb pseudopotential. In Fig. 3(c), we compare the dependence of T_c on Ω_{pl} as obtained under the two different physical situations. We clearly see that T_c from Eq. (31) is lower than the one from Eq. (32), owing to the absence of the dynamical electron correlation effect. We also note that the present system is on the BCS side of the BCS-BEC crossover [61,62], and is of the generalized BCS type, not only because of the nonadiabatic nature of the EPHC, but also due to the cooperative effects of the EPHC and EPLC in mediating electron pairing.

Beyond the estimated T_c , the present “phonon + plasmon” picture also provides new angels to further understand other related properties of the studied system. First, one pronounced feature of the multichannel pairing is the weaker isotope effect, as expected from Eq. (31) or (32), yielding $\alpha = \lambda_{\text{ph}}/2(\lambda_{\text{tot}} - \mu^*(1 + \lambda_{\text{tot}})) < 1/2$. This finding is qualitatively consistent with existing experimental observations [63]. Secondly, an intriguing replica band has been experimentally observed in 1uc-FeSe/STO, yet its underlying physical origin is still under active debate [16,18,29]. The prevailing picture is based on the electron-boson forward scattering mechanism, even though the responsible bosonic mode is unsettled. Based on the present study of the “phonon + plasmon” mechanism, the plasmon mode can naturally give rise to an additional replica band within the forward scattering mechanism associated with its long wavelength. Potential existence of such a weaker plasmon-based replica band below the phonon-based replica band might even have been seen experimentally (see Fig. 4 in Ref. [16]). Collectively, the concerted “phonon + plasmon” mechanism offers new angels to understand the different manifestations of 1uc-FeSe/STO as a high- T_c superconductor, and some of our unique predictions can be tested in future control experiments.

VI. DISCUSSION AND CONCLUSION

Before closing, we wish to stress the general applicability of the plasmon enhanced superconductivity theory presented in this work. In particular, the EPLC mechanism should always play an important role in systems with low effective carrier densities. Such systems, including other properly doped superconductors with FeSe as the elemental superconducting blocks [11,12,64–68], alkali-

metal-doped C₆₀ compounds [69,70], and even the Cu-based superconductors [1–3], share the striking commonality: All with very low carrier densities even at optimal doping defined by the highest T_c . Such low carrier densities are demanded by the metallicity nature of the systems in the normal states, and are simultaneously also accompanied by low energy plasmons, thereby providing the foundation of the “phonon + plasmon” mechanism to be operative. It is therefore highly desirable to generalize this mechanism to other related system with effective low carrier densities at a quantitative level, a task for future studies.

Within the main objective of the present study, we have focused on conveying the vital physics of low energy plasmon mode and the frequency dependent Coulomb repulsion in enhancing the superconductivity when join force with a phonon mode, especially when applied to the 1uc-FeSe/STO system. In doing so, some approximations are necessarily adopted, and errors in the range of a few Kelvin are introduced correspondingly into the obtained T_c . Such errors are tolerable at the present stage, especially given the vital finding that the “plasmon + phonon” mechanism can enhance the T_c by one order of magnitude to the experimentally observed range. We expect more accurate evaluations of the T_c will be achieved as field further advances.

In conclusion, our work reveled for the first time the crucial role of low energy plasmons in enhancing electron pairing in 1uc-FeSe/STO, especially with the EPHC and EPLC treated on equal footing. We found that, whereas the EPHC mechanism alone could only yield a low T_c of a few Kelvin, its constructive interplay with the EPLC is able to produce a strikingly large enhancement of T_c to tens of Kelvin. Moreover, we expect that the characteristic dependences of T_c on the plasmon frequency and isotope substitution can serve as important guides in future experimental studies, and the generic “phonon + plasmon” theory to be broadly applicable to many superconducting systems possessing low carrier densities and accordingly low energy optical plasmon modes. In particular, we expect the present study will also shed new light on the eventual identification of the dominant microscopic mechanism(s) of Cu-based superconductors.

ACKNOWLEDGMENTS

We thank Jiandong Guo, Dr. Wei Qin, and Zhongxian Zhao for insightful discussions. This work is supported by the National Natural Science Foundation of China (Grants No. 11634011 and No. 61434002), the National Key R&D Program of China (Grant No. 2017YFA0303500), and the Anhui Initiative in Quantum Information Technologies (Grant No. AHY170000).

APPENDIX A: ESTIMATION ON THE EPLC STRENGTH

We follow the work of Lundqvist [71,72], who studied the EPLC in a degenerate electron gas and predicted the plasmon-based satellite band in the single-particle spectrum induced by the EPLC. In his derivations, the general EPLC matrix element g_q is expressed as

$$|g_q|^2 = \frac{V(q)}{\left. \frac{\partial \epsilon(q, \omega)}{\partial \omega} \right|_{\omega=\omega_{\text{pl}}}}, \quad (\text{A1})$$

where $\epsilon(q, \omega)$ is the dielectric function, $V(q) = e^2/(\Omega \epsilon_0 q^2)$ is the Coulomb repulsion, and ϵ_0 is the static dielectric constant. Given that the superconducting gap in 1uc-FeSe/STO is largely isotropic [9,44], the EPLC matrix element can be treated as a constant [73]

$$\left(\frac{g}{\Omega_{\text{pl}}} \right)^2 = \frac{1}{\epsilon_0} \frac{e^2 q_0}{\pi \Omega_{\text{pl}}}, \quad (\text{A2})$$

here, q_0 is the radius of the spherical Brillouin zone.

To estimate the EPLC strength in 1uc-FeSe/STO from Eq. (A2), ϵ_0 is derived from the expression for the density dependence of the plasmon frequency $\Omega_{\text{pl}} = (4\pi e^2 n / \epsilon_0 m^*)^{1/2}$, where n is the electron density, and m^* is the electron effective mass. The electron density n is estimated to be $2.9 \times 10^{21} \text{ cm}^{-3}$ using $0.12 e^-$ per Fe atom in the FeSe monolayer, as measured experimentally [10]. The effective electron mass is estimated to be $m^* \sim 3m_0$ by fitting the band dispersion from experimental observations [10]. Given the plasmon frequency in the main text, we have $\epsilon_0 \sim 45.468$. Finally, we chose $q_0 = 4k_{\text{F}}$ to approximate the Brillouin zone containing two iron atoms in 1uc-FeSe/STO, and obtain $(g/\Omega_{\text{pl}})^2 \sim 0.518$. Then, we can derive the EPLC strength $\lambda_{\text{pl}}(k)$ by the following expression

$$\lambda_{\text{pl}}(k) = \frac{2V}{(2\pi)^3} \int_0^{q_0} \frac{d^2 p}{v_F} \frac{|g(k-p)|^2}{\Omega_{\text{pl}}(k-p)}. \quad (\text{A3})$$

Here, V is the volume of the unit cell of the monolayered FeSe. Since the isotropic approximation is adopted, we have

$$\lambda_{\text{pl}} = \lambda_{\text{pl}}(k) = \frac{2V}{(2\pi)^3} \cdot \frac{\pi g^2 q_0^2}{v_F \Omega_{\text{pl}}} \sim 0.25, \quad (\text{A4})$$

where v_F is the Fermi velocity. It is worthwhile to emphasize that $\lambda_{\text{pl}} \propto (g^2/\Omega_{\text{pl}}) = e^2 q_0 / (\pi \epsilon_0)$ is independent of the electron density, as ϵ_0 is unchanged when the electron density is varied.

APPENDIX B: DETERMINATION OF THE TRUNCATION FREQUENCY Ω_{cut}

To self-consistently solve the Eliashberg equations, it is necessary to truncate the summation over the Matsubara frequency of the electrons. In traditional systems, the typical energy associated with Ω_{cut} is on the order of 1 eV, set as four to ten times of the largest phonon frequency [74,75]. Here, when we examine the convergence of T_c on Ω_{cut} in 1uc-FeSe/STO, we find the T_c evolution with Ω_{cut} exhibits intriguing new features, as discussed below. In Fig. 4(a), we first show the T_c evolution with Ω_{cut} using the interaction kernel

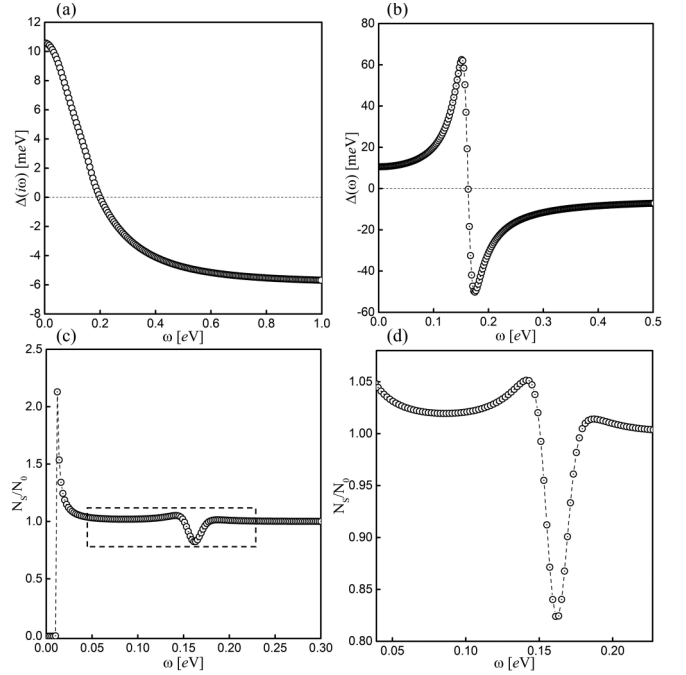


FIG. 5. (a) Gap function along the imaginary frequency axis at $T = 2.5$ K. (b) Real part of the gap function on the real frequency axis obtained by the Páde approximation from (a). (c) The corresponding normalized DOS in the superconducting state. (d) Magnified region near the boson (phonon and plasmon) frequencies, as indicated by the rectangle in (c).

$K(i\omega) = \mu^*(0) - \lambda_{\text{tot}}(i\omega)$, in which the Coulomb pseudopotential is in its static limit. We find T_c increases with Ω_{cut} slowly and converges within the typical range of $(5 - 10)\Omega_{\text{pl}}$, as traditionally expected. Figure 4(c) further shows the strikingly contrast T_c evolution when the dynamical nature of the Coulomb pseudopotential $\mu^*(\omega)$ is explicitly considered. Here, T_c decreases inversely with Ω_{cut} rapidly and converges around $\Omega_{\text{cut}} \sim 15\Omega_{\text{pl}}$.

The above contrast features can be qualitatively understood as follows. As we know, not all the electrons within the Fermi window can form Cooper pairs and directly contribute to the superconductivity. This is reflected by the fact that the interaction between some electrons within the Fermi window is still repulsive, preventing their pairing. As a result, the gap function $\Delta(\omega)$ will have both positive and negative parts along the frequency axis [53]. When specified to the present case, as shown in Figs. 4(b) and 4(d), the "sign-changing" structure of $\Delta(\omega)$ correlates with the total e-e interaction strength [or the interaction kernel $K(\omega)$ defined in the main text] on the frequency axis. Importantly, the Coulomb repulsion can scatter the electrons from one regime defined by a specific gap sign to another regime with the opposite gap sign, but such scattering processes are imbalanced, in that on average more electrons are scattered from the negative gap regime with strong Coulomb repulsion to the positive gap regime with net e-e attraction. Such frequency-dependent scattering processes are labeled as the dynamical electron correlation effect in Ref. [53].

When comparing Figs. 4(a) with 4(c) at the same Ω_{cut} , the obtained T_c is increased in the latter case due to the stronger

Coulomb pseudopotential at high frequencies, which leads to a larger scattering probability and a higher T_c accordingly. In the static case, increasing the cutoff energy could enlarge the contribution of the above scattering processes, resulting in the slowly increasing T_c shown in Fig. 4(a). On the contrary, in the dynamical case, T_c now decreases with Ω_{cut} , caused by the decreased Coulomb pseudopotential at $\omega > \Omega_{\text{pl}}$ [see Eq. (21)].

APPENDIX C: SUPERCONDUCTING GAP FUNCTION ON THE REAL FREQUENCY AXIS

In Fig. 5(a), we show the superconducting gap function $\Delta_{i\omega}$ solved on the imaginary frequency axis at $T = 2.5$ K and then continue it to the real frequency axis by the Páde approximation shown in Fig. 5(b) [74]. Clearly,

the superconducting gaps at the Fermi level obtained on the imaginary and real frequency axis agree with each other. The broad peak emerging in Fig. 5(b) indicates the energy scale of the boson frequencies [75]. Furthermore, we can obtain the normalized density of states (DOS) in the superconducting state as $N_S(\omega)/N_0$ from the gap function on the real axis by $N_S(\omega)/N_0 = \text{Re}[\omega/\sqrt{\omega^2 - \Delta^2(\omega)}]$, where N_0 is the DOS at the Fermi level in the normal state, and the result is shown in Fig. 5(c). The strong Van Hove singularity highlights the leading edge $\Delta_0 = 10.5$ meV for the superconducting gap in 1uc-FeSe/STO at the optimal doping. The DOS near the boson frequencies is magnified in Fig. 5(d). The fine structure signifies the electron-boson coupling and may provide a basis for direct measurement of the Eliashberg spectral function using tunneling spectroscopy [76].

-
- [1] J. G. Bednorz and K. A. Müller, Possible high T_c superconductivity in the Ba-La-Cu-O system, *Z. Phys. B* **64**, 189 (1986).
- [2] A. Damascelli, Z. Hussain, and Z.-X. Shen, Angle-resolved photoemission studies of the cuprate superconductors, *Rev. Mod. Phys.* **75**, 473 (2003).
- [3] I. Bozovic, X. He, J. Wu, and A. T. Bollinger, Dependence of the critical temperature in overdoped copper oxides on superfluid density, *Nature (London)* **536**, 309 (2016).
- [4] Y. Kamihara, H. Hiramatsu, M. Hirano, R. Kawamura, H. Yanagi, T. Kamiya, and H. Hosono, Iron-based layered superconductor: LaOFeP, *J. Am. Chem. Soc.* **128**, 10012 (2006).
- [5] Y. Kamihara, T. Watanabe, M. Hirano, and H. Hosono, Iron-based layered superconductor $\text{La}[\text{O}_{1-x}\text{F}_x]\text{FeAs}$ ($x=0.05-0.12$) with $T_c = 26$ K, *J. Am. Chem. Soc.* **130**, 3296 (2008).
- [6] X. H. Chen, T. Wu, G. Wu, R. H. Liu, H. Chen, and D. F. Fang, Superconductivity at 43 K in $\text{SmFeAsO}_{1-x}\text{F}_x$, *Nature (London)* **453**, 761 (2008).
- [7] F. C. Hsu, J.-Y. Luo, K.-W. Yeh, T.-K. Chen, T.-W. Huang, P. M. Wu, Y.-C. Lee, Y.-L. Huang, Y.-Y. Chu, D.-C. Yan, and M.-K. Wu, Superconductivity in the PbO-type structure α -FeSe, *Proc. Natl. Acad. Sci. USA* **105**, 14262 (2008).
- [8] Q.-Y. Wang, Z. Li, W.-H. Zhang, Z.-C. Zhang, J.-S. Zhang, W. Li, H. Ding, Y.-B. Ou, P. Deng, K. Chang, J. Wen, C. L. Song, K. He, J. F. Jia, S. H. Ji, Y. Y. Wang, L. L. Wang, X. Chen, X. C. Ma, and Q. K. Xue, Interface-induced high-temperature superconductivity in single unit-cell FeSe films on SrTiO_3 , *Chin. Phys. Lett.* **29**, 037402 (2012).
- [9] D. Liu, W. Zhang, D. Mou, J. He, Y. B. Ou, Q. Y. Wang, Z. Li, L. Wang, L. Zhao, S. He, Y. Peng, X. Liu, C. Chen, L. Yu, G. Liu, X. Dong, J. Zhang, C. Chen, Z. Xu, J. Hu, and Q. Xue, Electronic origin of high-temperature superconductivity in single-layer FeSe superconductor, *Nat. Commun.* **3**, 931 (2012).
- [10] S. He, J. He, W. Zhang, L. Zhao, D. Liu, X. Liu, D. Mou, Y. B. Ou, Q. Y. Wang, Z. Li, L. Wang, Y. Peng, Y. Liu, C. Chen, L. Yu, G. Liu, X. Dong, J. Zhang, C. Chen, and Z. Xu, Phase diagram and electronic indication of high-temperature superconductivity at 65 K in single-layer FeSe films, *Nat. Mater.* **12**, 605 (2013).
- [11] X. F. Lu, N. Z. Wang, H. Wu, Y. P. Wu, D. Zhao, X. Z. Zeng, X. G. Luo, T. Wu, W. Bao, G. H. Zhang, F. Q. Huang, Q. Z. Huang, and X. H. Chen, Coexistence of superconductivity and antiferromagnetism in $(\text{Li}_{0.8}\text{Fe}_{0.2})\text{OHFeSe}$, *Nat. Mater.* **14**, 325 (2015).
- [12] U. Pachmayr, F. Nitsche, H. Luetkens, S. Kamusella, F. Bruckner, R. Sarkar, H. H. Klauss, and D. Johrendt, Coexistence of 3d-ferromagnetism and superconductivity in $[(\text{Li}_{1-x}\text{Fex})\text{OH}](\text{Fe}_{1-y}\text{Li}_y)\text{Se}$, *Angew. Chem., Int. Ed. Engl.* **54**, 293 (2015).
- [13] J. Bardeen, L. N. Cooper, and J. R. Schrieffer, Theory of superconductivity, *Phys. Rev.* **108**, 1175 (1957).
- [14] S. Tan, Y. Zhang, M. Xia, Z. Ye, F. Chen, X. Xie, R. Peng, D. Xu, Q. Fan, H. Xu, J. Jiang, T. Zhang, X. Lai, T. Xiang, J. Hu, B. Xie, and D. Feng, Interface-induced superconductivity and strain-dependent spin density waves in FeSe/SrTiO₃ thin films, *Nat. Mater.* **12**, 634 (2013).
- [15] H. Y. Cao, S. Tan, H. Xiang, D. L. Feng, and X. G. Gong, Interfacial effects on the spin density wave in FeSe/SrTiO₃ thin films, *Phys. Rev. B* **89**, 014501 (2014).
- [16] J. J. Lee, F. T. Schmitt, R. G. Moore, S. Johnston, Y. T. Cui, W. Li, M. Yi, Z. K. Liu, M. Hashimoto, Y. Zhang, D. H. Lu, T. P. Devereaux, D. H. Lee, and Z. X. Shen, Interfacial mode coupling as the origin of the enhancement of T_c in FeSe films on SrTiO₃, *Nature (London)* **515**, 245 (2014).
- [17] C. Liu, Z. Wang, S. Ye, C. Chen, Y. Liu, Q. Wang, Q. H. Wang, and J. Wang, Detection of bosonic mode as a signature of magnetic excitation in one-unit-cell FeSe on SrTiO₃, *Nano. Lett.* **19**, 3464 (2019).
- [18] S. Zhang, T. Wei, J. Guan, Q. Zhu, W. Qin, W. Wang, J. Zhang, E. W. Plummer, X. Zhu, Z. Zhang, and J. Guo, Enhanced Superconducting State in FeSe/SrTiO₃ by a Dynamic Interfacial Polaron Mechanism, *Phys. Rev. Lett.* **122**, 066802 (2019).
- [19] E. Dagotto, Colloquium: The unexpected properties of alkali metal iron selenide superconductors, *Rev. Mod. Phys.* **85**, 849 (2013).
- [20] I. Bozovic and C. Ahn, A new frontier for superconductivity, *Nat. Phys.* **10**, 892 (2014).
- [21] H. Hosono and K. Kuroki, Iron-based superconductors: Current status of materials and pairing mechanism, *Physica C* **514**, 399 (2015).

- [22] D.-H. Lee, Routes to high-temperature superconductivity: A lesson from FeSe/SrTiO₃, *Annu. Rev. Condens. Matter Phys.* **9**, 261 (2018).
- [23] N. N. Bogoliubov, V. V. Tolmachev, and D. V. Shirkov, *A New Method in the Theory of Superconductivity* (Consultant Bureau, New York, 1959).
- [24] P. Morel and P. W. Anderson, Calculation of the superconducting state parameters with retarded electron-phonon interaction, *Phys. Rev.* **125**, 1263 (1962).
- [25] S. Zhang, J. Guan, X. Jia, B. Liu, W. Wang, F. Li, L. Wang, X. Ma, Q. Xue, J. Zhang, E. W. Plummer, X. Zhu, and J. Guo, Role of SrTiO₃ phonon penetrating into thin FeSe films in the enhancement of superconductivity, *Phys. Rev. B* **94**, 081116(R) (2016).
- [26] L. Rademaker, Y. Wang, T. Berlijn, and S. Johnston, Enhanced superconductivity due to forward scattering in FeSe thin films on SrTiO₃ substrates, *New J. Phys.* **18**, 022001 (2016).
- [27] W. H. Zhang, X. Liu, C. H. Wen, R. Peng, S. Y. Tan, B. P. Xie, T. Zhang, and D. L. Feng, Effects of surface electron doping and substrate on the superconductivity of epitaxial FeSe films, *Nano. Lett.* **16**, 1969 (2016).
- [28] S. N. Rebec, T. Jia, C. Zhang, M. Hashimoto, D. H. Lu, R. G. Moore, and Z. X. Shen, Coexistence of Replica Bands and Superconductivity in FeSe Monolayer Films, *Phys. Rev. Lett.* **118**, 067002 (2017).
- [29] F. Li and G. A. Sawatzky, Electron Phonon Coupling Versus Photoelectron Energy Loss at the Origin of Replica Bands in Photoemission of FeSe on SrTiO₃, *Phys. Rev. Lett.* **120**, 237001 (2018).
- [30] L. P. Gor'kov, Superconducting transition temperature: Interacting Fermi gas and phonon mechanisms in the nonadiabatic regime, *Phys. Rev. B* **93**, 054517 (2016).
- [31] B. Rosenstein and B. Y. Shapiro, High-temperature superconductivity in single unit cell layer FeSe due to soft phonons in the interface layer of the SrTiO₃ substrate, *Phys. Rev. B* **100**, 054514 (2019).
- [32] A. Aperis and P. M. Oppeneer, Multiband full-bandwidth anisotropic Eliashberg theory of interfacial electron-phonon coupling and high- T_c superconductivity in FeSe/SrTiO₃, *Phys. Rev. B* **97**, 060501(R) (2018).
- [33] T. P. Devereaux, T. Cuk, Z. X. Shen, and N. Nagaosa, Anisotropic Electron-Phonon Interaction in the Cuprates, *Phys. Rev. Lett.* **93**, 117004 (2004).
- [34] A. S. Mishchenko and N. Nagaosa, Electron-Phonon Coupling and a Polaron in the t-J Model: From the Weak to the Strong Coupling Regime, *Phys. Rev. Lett.* **93**, 036402 (2004).
- [35] N. P. Armitage, P. Fournier, and R. L. Greene, Progress and perspectives on electron-doped cuprates, *Rev. Mod. Phys.* **82**, 2421 (2010).
- [36] H. Fröhlich, Superconductivity in Metals with Incomplete Inner Shells, *J. Phys. C* **1**, 544 (1968).
- [37] Y. Takada, Plasmon mechanism of superconductivity in two- and three-dimensional electron systems, *J. Phys. Soc. Jpn.* **45**, 3 (1978).
- [38] R. Akashi and R. Arita, Development of Density-Functional Theory for a Plasmon-Assisted Superconducting State: Application to Lithium under High Pressures, *Phys. Rev. Lett.* **111**, 057006 (2013).
- [39] I. Bozovic, Plasmons in cuprate superconductors, *Phys. Rev. B* **42**, 1969 (1990).
- [40] N. Reyren, S. Thiel, A. D. Caviglia, L. F. Kourkoutis, G. Hammerl, C. Richter, C. W. Schneider, T. Kopp, A.-S. Rüetschi, D. Jaccard, M. Gabay, D. A. Muller, J.-M. Triscone, and J. Mannhart, Superconducting interfaces between insulating oxides, *Science* **317**, 1196 (2007).
- [41] R. M. Fernandes, J. T. Haraldsen, P. Wölfle, and A. V. Balatsky, Two-band superconductivity in doped SrTiO₃ films and interfaces, *Phys. Rev. B* **87**, 014510 (2013).
- [42] M. N. Gastiasoro, A. V. Chubukov, and R. M. Fernandes, Phonon-mediated superconductivity in low carrier-density systems, *Phys. Rev. B* **99**, 094524 (2019).
- [43] M. N. Gastiasoro, J. Ruhman, and R. M. Fernandes, Superconductivity in dilute SrTiO₃: A review, *Ann. Phys.* **417**, 168107 (2020).
- [44] Q. Fan, W. H. Zhang, X. Liu, Y. J. Yan, M. Q. Ren, R. Peng, H. C. Xu, B. P. Xie, J. P. Hu, T. Zhang, and D. L. Feng, Plain s-wave superconductivity in single-layer FeSe on SrTiO₃ probed by scanning tunnelling microscopy, *Nat. Phys.* **11**, 946 (2015).
- [45] W. E. Pickett, Generalization of the theory of the electron-phonon interaction: Thermodynamic formulation of superconducting- and normal-state properties, *Phys. Rev. B* **26**, 1186 (1982).
- [46] F. Giustino, Electron-phonon interactions from first principles, *Rev. Mod. Phys.* **89**, 015003 (2017).
- [47] A. B. Migdal, Interaction between electrons and lattice vibrations in a normal metal, *Sov. Phys. JETP* **34**, 996 (1958).
- [48] C. Grimaldi, L. Pietronero, and S. Strassler, Nonadiabatic Superconductivity: Electron-Phonon Interaction Beyond Migdal's Theorem, *Phys. Rev. Lett.* **75**, 1158 (1995).
- [49] G. D. Mahan, *Many-Particle Physics* (Kluwer Academic, New York, 2000).
- [50] J. T. Devreese, S. N. Klimin, J. L. M. van Mechelen, and D. van der Marel, Many-body large polaron optical conductivity in SrTi_{1-x}Nb_xO₃, *Phys. Rev. B* **81**, 125119 (2010).
- [51] K. Sano, M. Seo, and K. Nakamura, Plasmon Effect on the Coulomb Pseudopotential μ^* in the McMillan Equation, *J. Phys. Soc. Jpn.* **88**, 093703 (2019).
- [52] H. Rietschel and L. J. Sham, Role of electron Coulomb interaction in superconductivity, *Phys. Rev. B* **28**, 5100 (1983).
- [53] D. J. Scalapino, A common thread: The pairing interaction for unconventional superconductors, *Rev. Mod. Phys.* **84**, 1383 (2012).
- [54] B. Li, Z. W. Xing, G. Q. Huang, and D. Y. Xing, Electron-phonon coupling enhanced by the FeSe/SrTiO₃ interface, *J. Appl. Phys.* **115**, 193907 (2014).
- [55] Y. C. Tian, W. H. Zhang, F. S. Li, Y. L. Wu, Q. Wu, F. Sun, G. Y. Zhou, L. Wang, X. Ma, Q. K. Xue, and J. M. Zhao, Ultrafast Dynamics Evidence of High Temperature Superconductivity in Single Unit Cell FeSe on SrTiO₃, *Phys. Rev. Lett.* **116**, 107001 (2016).
- [56] B. Rosenstein, B. Y. Shapiro, I. Shapiro, and D. Li, Superconductivity in the two-dimensional electron gas induced by high-energy optical phonon mode and large polarization of the SrTiO₃ substrate, *Phys. Rev. B* **94**, 024505 (2016).
- [57] W. L. McMillan, Transition temperature of strong-coupled superconductors, *Phys. Rev.* **167**, 331 (1968).
- [58] S. Coh, M. L. Cohen, and S. G. Louie, Large electron-phonon interactions from FeSe phonons in a monolayer, *New J. Phys.* **17**, 073027 (2015).

- [59] X. Li, D. Xiao, and Z. Zhang, Landau damping of quantum plasmons in metal nanostructures, *New J. Phys.* **15**, 023011 (2013).
- [60] G. Cheng, W. Qin, M.-H. Lin, L. Wei, X. Fan, H. Zhang, S. Gwo, C. Zeng, J. G. Hou, and Z. Zhang, Substantially Enhancing Quantum Coherence of Electrons in Graphene via Electron-Plasmon Coupling, *Phys. Rev. Lett.* **119**, 156803 (2017).
- [61] F. Schrodri, A. Aperis, and P. M. Oppeneer, Self-consistent temperature dependence of quasiparticle bands in monolayer FeSe on SrTiO₃, *Phys. Rev. B* **98**, 094509 (2018).
- [62] S. Zhang, G. Miao, J. Guan, X. Xu, B. Liu, F. Yang, W. Wang, X. Zhu, and J. Guo, Superconductivity of the FeSe/SrTiO₃ interface in view of BCS-BEC crossover, *Chin. Phys. Lett.* **36**, 107404 (2019).
- [63] Q. Song, T. L. Yu, X. Lou, B. P. Xie, H. C. Xu, C. H. P. Wen, Q. Yao, S. Y. Zhang, X. T. Zhu, J. D. Guo, R. Peng, and D. L. Feng, Evidence of cooperative effect on the enhanced superconducting transition temperature at the FeSe/SrTiO₃ interface, *Nat. Commun.* **10**, 758 (2019).
- [64] S. Kasahara, T. Watashige, T. Hanaguri, Y. Kohsaka, T. Yamashita, Y. Shimoyama, Y. Mizukami, R. Endo, H. Ikeda, K. Aoyama, T. Terashima, S. Uji, T. Wolf, H. von Lohneysen, T. Shibauchi, and Y. Matsuda, Field-induced superconducting phase of FeSe in the BCS-BEC cross-over, *Proc. Natl. Acad. Sci. USA* **111**, 16309 (2014).
- [65] X. Liu, L. Zhao, S. He, J. He, D. Liu, D. Mou, B. Shen, Y. Hu, J. Huang, and X. J. Zhou, Electronic structure and superconductivity of FeSe-related superconductors, *J. Phys.: Condens. Matter* **27**, 183201 (2015).
- [66] B. Lei, J. H. Cui, Z. J. Xiang, C. Shang, N. Z. Wang, G. J. Ye, X. G. Luo, T. Wu, Z. Sun, and X. H. Chen, Evolution of High-Temperature Superconductivity from a Low- T_c Phase Tuned by Carrier Concentration in FeSe Thin Flakes, *Phys. Rev. Lett.* **116**, 077002 (2016).
- [67] C. L. Song, H. M. Zhang, Y. Zhong, X. P. Hu, S. H. Ji, L. Wang, K. He, X. C. Ma, and Q. K. Xue, Observation of Double-Dome Superconductivity in Potassium-Doped FeSe Thin Films, *Phys. Rev. Lett.* **116**, 157001 (2016).
- [68] L. Zhao, A. Liang, D. Yuan, Y. Hu, D. Liu, J. Huang, S. He, B. Shen, Y. Xu, X. Liu, L. Yu, G. Liu, H. Zhou, Y. Huang, X. Dong, F. Zhou, K. Liu, Z. Lu, Z. Zhao, C. Chen *et al.*, Common electronic origin of superconductivity in (Li, Fe)OHFeSe bulk superconductor and single-layer FeSe/SrTiO₃ films, *Nat. Commun.* **7**, 10608 (2016).
- [69] O. Gunnarsson, Superconductivity in fullerenes, *Rev. Mod. Phys.* **69**, 575 (1997).
- [70] W. L. Yang, V. Brouet, X. J. Zhou, H. J. Choi, S. G. Louie, M. L. Cohen, S. A. Kellar, P. V. Bogdanov, A. Lanzara, A. Goldoni, F. Parmigiani, Z. Hussain, and Z.-X. Shen, Band structure and fermi surface of electron-doped C₆₀ monolayers, *Science* **300**, 303 (2003).
- [71] B. I. Lundqvist, Single-particle spectrum of the degenerate electron gas, *Phys. Kondens. Mater.* **6**, 193 (1967).
- [72] B. I. Lundqvist, Single-particle spectrum of the degenerate electron gas, *Phys. Kondens. Mater.* **6**, 206 (1967).
- [73] V. P. Antropov, O. Gunnarsson, and A. I. Liechtenstein, Phonons, electron-phonon, and electron-plasmon coupling in C60 compounds, *Phys. Rev. B* **48**, 7651 (1993).
- [74] H. J. Vidberg and J. W. Serene, Solving the eliashberg equations by means of pade approximants, *J. Low Temp. Phys.* **29**, 179 (1977).
- [75] E. R. Margine and F. Giustino, Anisotropic migdal-eliashberg theory using wannier functions, *Phys. Rev. B* **87**, 024505 (2013).
- [76] C. L. Song, Y. L. Wang, Y. P. Jiang, Z. Li, L. Wang, K. He, X. Chen, J. E. Hoffman, X. C. Ma, and Q. K. Xue, Imaging the Electron-Boson Coupling in Superconducting FeSe Films using a Scanning Tunneling Microscope, *Phys. Rev. Lett.* **112**, 057002 (2014).